Synthesis, Polymorphs, and Luminescent Properties of Oligomeric Zn_3ppo_6

T. S. Kim,* T. Okubo, and T. Mitani

Department of Physical Materials Science, Japan Advanced Institute of Science and Technology, 1-8, Asahidai, Tatsunokuchi, Ishikawa, Japan

Received July 17, 2003. Revised Manuscript Received October 2, 2003

Oligomeric Zn_3ppo_6, where ppo is 2-(2-hydroxyphenyl)-5-phenyl-1,3-oxazole, has been synthesized as a new blue-emitting material for organic light-emitting diodes (OLEDs). The electroluminescence maximum wavelength is 450 nm and the Commission Internationale de l'Eclairage (CIE) coordinates are $x = 0.15$, $y = 0.11$ for blue chromaticity. The luminance efficiency and the maximum luminance were about 1.3 lm/W at 6 V, 5.8 mA/cm^2 (139 cd/m^2), and 8140 cd/m^2 at 11.4 V. Zn_3ppo_6 shows two trimeric polymorphs and a monomeric structure at different sublimation temperatures.

Introduction

Luminescent organic metal complexes are a fascinating class of materials because of their potential for use in a broad range of applications such as organic light-emitting devices (OLEDs), lasers, transistors, and fluorescent sensors for highly specific probes. Particularly great progress has been made in the development of OLEDs with low power consumption, excellent emissive qualities, and wide viewing angle. However, blue or white emitting materials remain the weakest link in realizing full-color OLED displays becaus of their low efficiency compared with that of green or red.[1−9]

The coordinative number of Zn complexes is changeable, making it possible to consider the creation of a new blue or multicolor emitter. Zinc complexes may have various molecular structures from monomer to polymer, as the coordination number of the zinc atom can range from 2 to 6. Therefore, Zn complex systems may show an oligomerization effect on their solid-state properties: their properties are different compared with those of monomeric structures. In addition, an oligomeric structure may give us a greater number of controllable parameters for designing a new system at the molecular level than could be achieved with a monomeric structure. As a result, these polynuclear complexes, apart from being of fundamental interest, can serve as model systems in the study of molecular-based functional materials.

Several Zn(II) complexes such as bis(8-hydroxyquinoline) Zn(II) (Znq_2), bis(2-(2-hydroxyphenyl)pyridine) Zn(II) ($Zn(PhPy)_2$), bis(2-(2-hydroxyphenyl)-5-phenyl-1,3,4-oxadizole) Zn(II) ($Zn(ODZ)_2$), bis(2-(2-hydroxy phenyl)-5-phenyl-1,3,4-thiadizole) Zn(II) ($Zn(TDZ)_2$), and bis(2-(2-hydroxyphenyl)thiazole) Zn(II) (Zn_2ptz_4) have been reported as potential OLED materials. However, each of these complexes has certain drawbacks when used for a practical OLED device.

The crystal structure of Znq_2 dihydrate has a distorted octahedral and monomeric structure,[10] whereas anhydrous Znq_2 prepared by a train sublimation method exists as only a tetrameric molecular structure including two different Zn(II) ion centers with 5- and 6-coordinated geometries, respectively.[11]

On the other hand, $Zn(PhPy)_2$, $Zn(ODZ)_2$, and $Zn(TDZ)_2$ show a red-shift of emission band or the appearance of a new peak at longer wavelengths when used in a device during continuous driving.[12]

Zn_2ptz_4 purified by a train sublimation method has a dimeric structure and shows two polymorphs at different sublimation temperatures, namely HT (high temperature)- and LT (low temperature)-Zn_2ptz_4.[13] The LT-polymorph shows a large energy shift in the emission band despite having the same absorption spectra as the HT-polymorph in solid state. These polymorphs have enabled the successful development of organic EL devices with blue and green emissions, suggesting the possibility of achieving a full-color EL display by controlling the polymorphs. However, elemental analy-

* To whom correspondence should be addressed. E-mail: taeshick@jaist.ac.jp.

(1) Aziz, H.; Popovic, Z. D.; Hu, N.-X.; Hor, A.-M.; Xu, G. *Science* **1999**, *283*, 1900.
(2) Kraft, A.; Grimsdale, A. C.; Holmes, A. B. *Angew. Chem., Int. Ed.* **1998**, *37*, 402.
(3) Bulovic, V.; Gu, G.; Burrows, P.; Forrest, V.; Thompson, N. E. *Nature* **1996**, *380*, 29.
(4) Sheats, J. R.; Antoniadis, H.; Hueschen, M.; Leonard, W.; Miller, J.; Moon, R.; Roitman, D.; Stocking, A. *Science* **1996**, *273*, 884.
(5) Kido, J.; Kimura, M.; Nagai, K. *Science* **1995**, *267*, 1332.
(6) Matsumi, N.; Naka, K.; Chujo, Y. *J. Am. Chem. Soc.* **1998**, *120*, 5112.
(7) Noda, T.; Shirota, Y.; Chuji, Y. *J. Am. Chem. Soc.* **1998**, *120*, 9714.
(8) Hassan, A.; Wang, S. *Chem. Commun.* **1998**, 211.
(9) Wu, Q.; Esteghamatian, M.; Hu, N.-X.; Popovic, Z.; Enright, G.; Breeze, S. R.; Wang, S. *Angew. Chem., Int. Ed.* **1999**, *38*, 985.
(10) Merritt, L. L.; Cady, R. T.; Mundy, B. W. *Acta Crystallogr.* **1954**, *7*, 473.
(11) Kai, Y.; Moraita, M.; Yasuka, N.; Kasai, N. *Bull. Chem. Soc. Jpn.* **1985**, *58*, 1631.
(12) Tokito, S.; Noda, K.; Tanaka, H.; Taga, Y.; Tsutsui, T. *Synth. Met.* **2000**, *111−112*, 393.
(13) Kim, T. S.; Knishii, K.; Ahn, J. S.; Okubo, T.; Mitani, T. *The 9th International Display Workshops*, 2002, *OEL 2−3*.

10.1021/cm0346428 CCC: $25.00
Published on Web 11/22/2003

Table 1. Crystal Data for M-Znppo$_2$, HT-Zn$_3$Ppo$_6$, and LT-Zn$_3$Ppo$_6$

empirical formula	$C_{30}N_2O_4Zn_1H_2$	$C_{90}N_6O_{12}Zn_3H_{60}$	$C_{90}N_6O_{12}Zn_3H_{60}$
crystal system	triclinic	monoclinic	triclinic
space group	$P\bar{1}$ (no. 2)	$P2_1/n$ (no. 14)	$P\bar{1}$ (no. 2)
a, Å	5.047	11.231	11.098
b, Å	13.337	14.782	11.382
c, Å	18.239	21.005	14.852
α, deg.	106.042	91.612	
β, deg.	90.111	91.053	105.740
γ, deg.	90.019	14.852	
V, Å^3	1180.0	3486.7	1742.6
Z	2	2	1
F(000)	552	1656	828
agreement indices	R1 = 0.090 Rw = 0.101	R1 = 0.023 Rw = 0.028	R1 = 0.068 Rw = 0.074

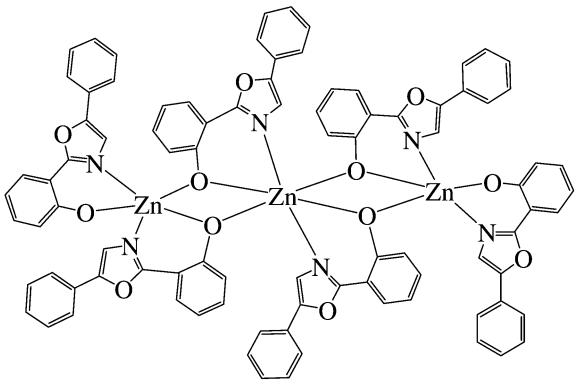

Figure 1. Chemical structure of Zn$_3$ppo$_6$.

ses, ^{13}C and ^{1}H NMR, and mass spectra could not distinguish them. Therefore, for practical materials, the crystal structure must be elucidated in order to predict or control the properties of thermally deposited thin films. Unfortunately, we could not elucidate the crystal structure of HT-polymorphs.

We anticipated that modifying the ptz ligand could give us the opportunity to elucidate the origin of the large emission band shift between different polymorphs. The new ligand we chose to investigate is 2-(2-hydroxyphenyl)-5-phenyl-1,3-oxazole (ppo). This paper describes the synthesis, polymorphs, and luminescent properties of Zn$_3$ppo$_6$. The chemical structure of the Zn$_3$ppo$_6$ ligand is presented in Figure 1.

Results and Discussion

This system, a Zn complex with ppo ligands, shows two oligomeric polymorphs and a very small amount (10−15 μg of needle-type crystals for the raw powder, 300 mg) of a monomeric one purified by a train sublimation method. They are named M-Znppo$_2$ (for the sample found at 280 °C), LT-Zn$_3$ppo$_6$ (310 °C), and HT-Zn$_3$ppo$_6$ (340 °C). M-Znppo$_2$ and LT-Zn$_3$ppo$_6$ are irreversibly converted to HT-Zn$_3$ppo$_6$ by a second sublimation under 10^{-3} Torr at 360 °C. The conversion of LT-Zn$_3$ppo$_6$ to HT-Zn$_3$ppo$_6$ is clearly shown in DSC traces. Figure 2 shows the DSC traces (at 10 °C/min) for the LT-Zn$_3$ppo$_6$ and HT-Zn$_3$ppo$_6$ samples. For the LT-Zn$_3$ppo$_6$ trace, the glass transition temperature (T_g) was observed to be about 235 °C. In subsequent heating and cooling scans, HT-Zn$_3$ppo$_6$ shows the relatively sharp crystallization temperature (T_c) at 327 °C. However, LT-Zn$_3$ppo$_6$ shows a shoulder at the low-temperature side (at about 311 °C), indicating an incomplete conversion to HT-Zn$_3$ppo$_6$.

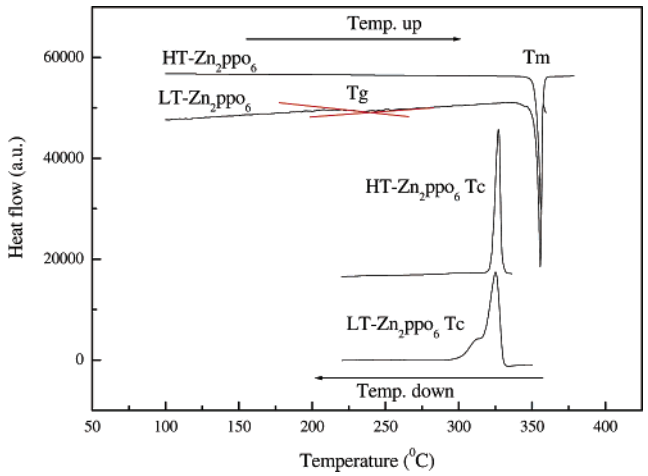

Figure 2. DSC traces for LT-Zn$_3$ppo$_6$ to HT-Zn$_3$ppo$_6$ samples.

Crystal Structure Analyses. The cell parameters of all crystalline systems observed in this study are summarized in Table 1. Their molecular packing structures and a trimeric molecular structure are presented in Figure 3. M-Znppo$_2$ exhibits 2D $\pi-\pi$ intermolecular packing, and both Zn$_3$ppo$_6$ systems show 3D $\pi-\pi$ stacking. The most favorable $\pi-\pi$ overlaps between facing ligands are found in LT-Zn$_3$ppo$_6$. The small intermolecular distances and orientations (oxygen atom of hydroxyphenyl and Zn atom between the neighboring molecules at [100] direction) of M-Znppo$_2$ molecules allow the oligomerization in solid state.

The LT-Zn$_3$ppo$_6$ to HT-Zn$_3$ppo$_6$ conversion is caused by the entropy effects resulting from variance of the torsion angles between three rings and the high rotational degree of freedom of the 5-positioned phenyl group. In fact, the two polymorphs have quite similar molecular structures except for the torsional angles between hydroxyphenyl, oxazole, and 5-positioned phenyl planes. Table 2 shows some selected bond lengths and bond angles.

Photoluminescence (PL). The oligomerization of the M-Znppo$_2$ to HT-Zn$_3$ppo$_6$ creates the blue-shifted PL spectrum from 470 to 440 nm at peak position. The PL spectrum is then significantly broadened without red shift by the well-defined 3D molecular packing of LT-Zn$_3$ppo$_6$ as shown in Figure 4.

This broadened PL spectrum is due to the cooperative interplay of the strong intermolecular interaction and flexible molecular structure in the LT-Zn$_3$ppo$_6$ crystal. Spectral broadening of the envelope of Franck−Condon transitions is commonly described by the linear coupling of the electronic states to the nuclear configuration. The

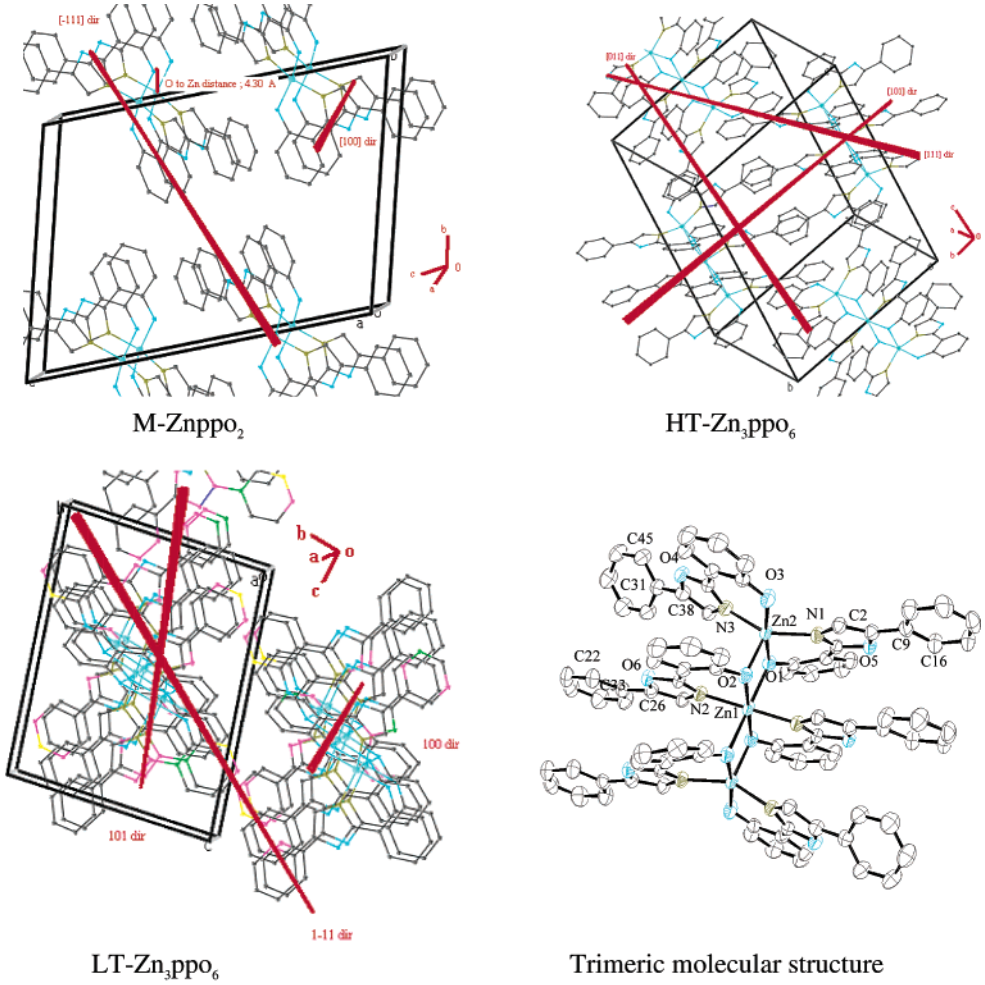

Figure 3. Molecular and packing structures in crystalline solid state. H atoms are omitted for clarity.

Table 2. Selected Bond Length, Bond Angle, and Torsion Angle for HT-Zn_3Ppo_6 and LT-Zn_3Ppo_6

	bond length (Å)			bond angle (°)			torsion angle (°)	
	HT	LT		HT	LT		HT	LT
Zn1−Zn2	3.169	3.180	Zn1−O1−Zn2	94.8	94.1	O1−Zn1−O2−Zn2	0.9	1.5
Zn1−O1	2.225	2.258	Zn1−O2−Zn2	100.4	101.3	N2−Zn1−O2−Zn2	93.9	94.8
Zn1−O2	2.074	2.077	O1−Zn1−O2	80.3	79.6	O3−Zn2−O1−Zn1	153.8	153.3
Zn2−O1	2.078	2.082	O1−Zn2−O2	84.5	84.9	N1−Zn2−Zn1-Z2	167.4	166.4
Zn2−O2	2.051	2.035	O1−Zn2−O3	171.9	173.7	N3−Zn2−Zn1−N2	13.2	13.9
Zn2−O3	1.998	2.003	O2−Zn2−O3	102.8	100.8	O3−Zn2−Zn1−N2	91.5	90.2
Zn1−N2	2.077	2.056	O2−Zn2−N3	104.2	104.9	O4−C38−C31−C45	28.7	18.0
Zn2−N1	2.038	2.033	O2−Zn2−N1	110.2	112.3	O5−C2−C9−C16	9.7	18.0
Zn2−N3	2.043	2.031	N1−Zn2−N3	145.5	142.6	O6−C26−C22−C33	1.6	2.8

intra-molecular vibrations, torsions, and positions of neighboring molecules can vary this nuclear configuration to a remarkable degree.

In addition, as shown in Figure 5, the same UV absorption spectra of two oligomeric polymorphs in thin film reflect different emissions, caused by different relaxation processes due to the packing effects.[14−15] We did not have enough M-$Znppo_2$ to investigate its UV absorption spectrum and EL properties.

Electroluminescence (EL). To investigate the EL characteristics of two polymorphs, some OLEDs were fabricated by the thermal evaporation method. The turn-on voltage of all devices used in this work was less than 5 V. The EL spectra of these OLEDs are illustrated in Figure 5.

The PL and EL spectra from evaporated LT-Zn_3ppo_6 thin film are different from those of a single crystal. From DSC results, these differences are caused by an incomplete LT- Zn_3ppo_6 to HT-Zn_3ppo_6 conversion. Voltage-dependent variance of the EL spectra from the LT-Zn_3ppo_6 device reflects the LT-Zn_3ppo_6 to HT-Zn_3ppo_6 conversion by Joule heat in an operated device as shown in Figure 6. However, devices 3 and 4 are not same as the HT-Zn_3ppo_6 devices. Consequently, the EL spectra of LT-Zn_3ppo_6 devices are attributed to the mixture of LT-Zn_3ppo_6 and HT-Zn_3ppo_6. This is the reason a color change occurred in the OLEDs.[12,16−20]

(14) DiCesare, N.; Belletete, M.; Marrano, C.; Leclerc, M.; Durocher, G. *J. Phys. Chem. A* **1999**, *103*, 803.
(15) Pope, M.; Swenberg, C. In *Electronic Processes in Organic Crystals and Polymers*; Oxford University Press: Oxford, U.K., 1999; p 56.

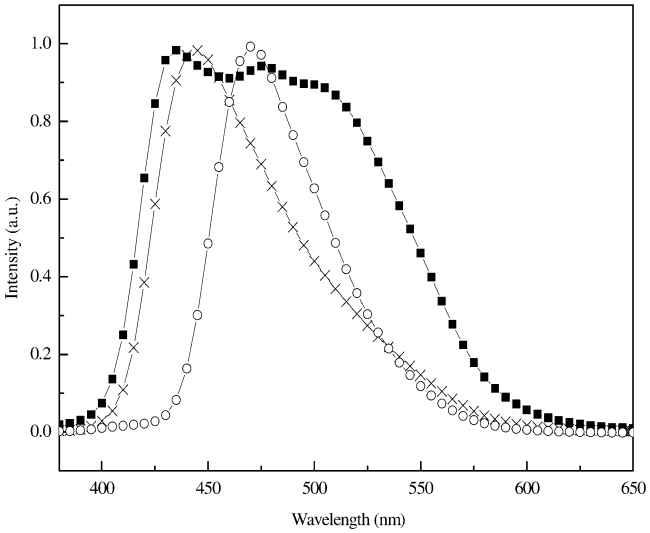

Figure 4. PL spectra of LT-Zn_3ppo_6 (-■-), HT-Zn_3ppo_6 (-×-), and M-$Znppo_2$ (-○-) single crystals.

For device 1, [ITO/TPD (50 nm)/HT-Zn_3ppo_6 (50 nm)/LiF (1 nm)/Al], the Commission Internationale de l'Eclairage (CIE) coordinates are $x = 0.15$, $y = 0.11$.

However, satisfactory performance from device 1 could not be achieved, although the EL spectrum observed was identical to that of device 2. The luminance efficiency is 0.008 lm/W at 8.3 mA/cm^2, 5 V, and 1 cd/m^2. Luminance−current density (L−J) and current density−voltage (J−V) characteristics are shown in Figure 7.

For device 2, [ITO/TPD (50 nm)/HT-Zn_3ppo_6 (45 nm)/PBD (5 nm)/LiF (1 nm)/Al], the CIE coordinates are $x = 0.15$, $y = 0.11$. The luminance efficiency is 1.26 lm/W at 5.8 mA/cm^2, 6 V, and 139 cd/m^2.

For device 3, [ITO/TPD (50 nm)/LT-Zn_3ppo_6 (45 nm)/PBD (5 nm)/LiF (1 nm)/Al], the luminance efficiency is 0.2 lm/W at 21 mA/cm^2, 6.9 V, and 90 cd/m^2.

In device 4, [ITO/TPD (48 nm)/HMB (2 nm)/LT-Zn_3ppo_6 (45 nm)/PBD (5 nm)/LiF (1 nm)/Al], the luminance efficiency is 1.29 lm/W at 8.97 mA/cm^2, 7.65 V, and 283 cd/m^2. Hexamethylbenzene (HMB), a chemically and optically inactive material (work function 7.85 eV),[21] was inserted for hole blocking, because a PBD layer thicker than 5 nm caused lower luminous efficiency and higher turn-on voltage.

The J−V characteristic of device 3 is quite similar to that of device 1, whereas that of device 4 is similar to that of device 2. Device 3 has a 5-nm PBD layer; device 4 has a 5-nm PBD layer and an additional 2-nm HMB layer. From these results, we can see that the low efficiency of device 3 is caused by the remaining LT-Zn_3ppo_6 structure with its strong intermolecular interactions, which cause favorable carrier transport. In this stage, however, we have a serious stress because we do not know how much LT-Zn_3ppo_6 structure remains in devices with the LT-Zn_3ppo_6 emitting layer.

Conclusions

$(Znppo_2)_n$ has been synthesized. This system shows two trimeric polymorphs and a monomeric structure at different sublimation temperatures. Monomeric $Znppo_2$ and LT-Zn_3ppo_6 are irreversibly converted to HT- Zn_3ppo_6 as shown in DSC traces and voltage-dependent EL spectra. The LT-Zn_3ppo_6 to HT- Zn_3ppo_6 conversion may be attributed to the high rotational degree of freedom of the 5-positioned phenyl group. Of course, a twist vibrational degree of freedom between three rings may also contribute LT-Zn_3ppo_6 to the HT-Zn_3ppo_6 conversion.

In an OLED using oligomeric HT-Zn_3ppo_6, the EL maximum wavelength is 450 nm and CIE coordinates are $x = 0.15$, $y = 0.11$ of blue chromaticity. The luminance efficiency and the maximum luminance were about 1.3 lm/W at 6 V, 5.8 mA/cm^2 (139 cd/m^2, internal quantum efficiency ~8.3%, refraction index ~1.788) and 8140 cd/m^2 at 11.4 V.

In addition, polymorphs should be controlled, since the existence of polymorphs could cause an unexpected property change in practical devices, specifically a color change in OLEDs, as shown in devices with a LT-Zn_3ppo_6 emitting layer.

Experimental Details

2-Methoxybenzoic acid and 2-amino-1-phenylethanol were purchased from TCI, and Aldrich Chemical Co., respectively. γ-Collidine, 1-hydroxybenzotriazole (HBT), and ethyldiisopropylamine were purchased from Nacalai tesque. From Kanto Chemical Co., *N*,*N*′-dicyclohexylcarbodiimide (DCC), triphenylphosphine, hexachloroethane, and triethyl-amine were purchased. Column chromatography was carried out on silica (silica gel 60, 70−230 mesh) to purify the ligand. ^{1}H NMR spectra were measured by a Varian FT-NMR GEMINI 2000 spectrometer to characterize the ligand. UV absorption spectra were recorded on a JASCO V-570 spectrometer. PL and EL spectra were recorded on a JASCO FP-6500 spectrometer. Samples were excited by a 365-nm UV light. The bandwidth of the light source was 3 nm. For the PL measurements of crystalline phases, an isolated single crystal was mounted on a quartz plate. The luminance−voltage−current density (L−V−J) characteristics were measured using a Topcon BM-8 luminance meter and a Keithley 2400 Source Meter.

In single-crystal X-ray analysis, all measurements were made on a Rigaku RAXIS imaging plate area detector with graphite monochromatic Mo Kα ($\lambda = 0.71073$ Å) radiation at 50 kV and 40 mA. The first sweep of data was using ω scans from 130.0 to 190.0° at $\chi = 45.0°$ and $\phi = 0.0°$. The detector is at the zero swing position. The crystal to detector distance was 127.40 mm. Readout was performed in the 0.100 mm pixel mode. The non-hydrogen atoms were refined anisotropically, while hydrogen atoms were refined isotropically. The structure was solved by a direct method (SIR97) and expanded using Fourier techniques (DIRDIF99) for all crystalline systems.

Synthesis of 2-[(2-Phenyl-2-hydroxyethyl)aminocarbonyl]ansiole. *o*-Anisic acid (8.2 g, 54 mmol), 1-hydroxybenzotriazole (HBT) (7.29 g, 54 mmol), ethyldiisopropylamine (10 mL, 54 mmol), 2-amino-1-phenylethanol (6.6 g, 48 mmol), and DCC (11.14 g, 54 mmol) were added to CH_2Cl_2 (300 mL), and then stirred for 5 h at room temperature. The mixture was cooled to 0 °C. The *N*, *N*′-dicyclohexylurea was filtered out. The filtrate was washed with saturated NH_4Cl aqueous solution and K_2CO_3 aqueous solution. The solvent was evaporated and then purified in a chromatographic column using

(16) Han, E.-M.; Do, L.-M.; Yamamoto, N.; Fujihira, M. *Thin Solid Films* **1996**, *273*, 202.
(17) Murata, H.; Merritt, C. D.; Inada, H.; Shirota, Y.; Kafafi, Z. H. *Appl. Phys. Lett.* **1999**, *75*, 3252.
(18) Tokito, S.; Tanaka, H.; Noda, K.; Okada, A.; Taga, Y. *Appl. Phys. Lett.* **1997**, *70*, 1929.
(19) Antoniadis, H.; Inbasekaran, M.; Woo, E. P. *Appl. Phys. Lett.* **1998**, *73*, 3055.
(20) Tamoto, N.; Adachi, C.; Nagai, K. *Chem. Mater.* **1997**, *9*, 1077.
(21) Rath, M. C.; Pal, H.; Mukherjee, T. *J. Phys. Chem. A* **2001**, *105*, 7945.

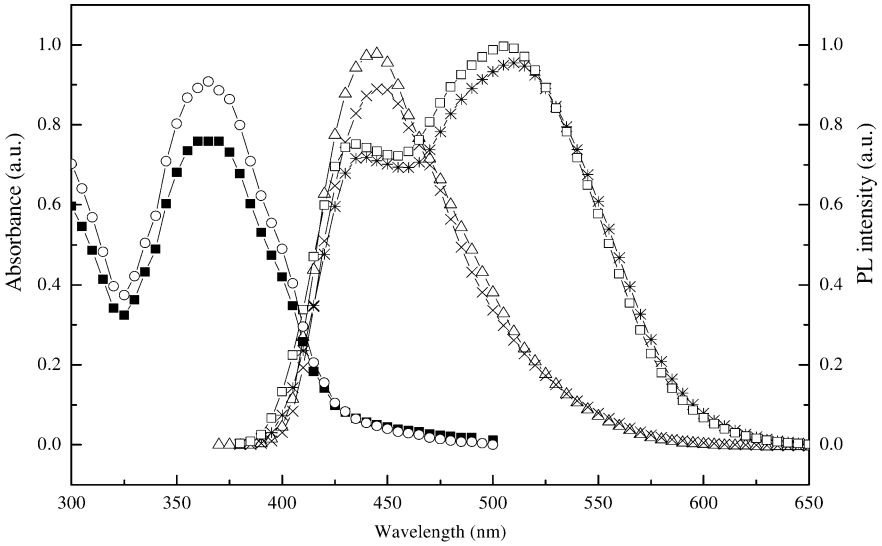

Figure 5. EL of HT-Zn_3ppo_6 based devices 1 and 2 (-×-), LT-Zn_3ppo_6 based devices 3 and 4 (-*-), thin film PL of HT-Zn_3ppo_6 (-△-) and LT-Zn_3ppo_6 (-□-), and thin film UV absorption spectra of HT-Zn_3ppo_6 (-■-) and LT-Zn_3ppo_6 (-○-).

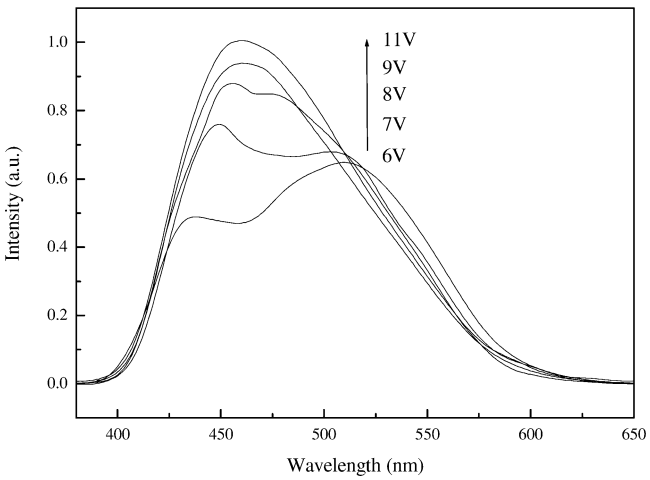

Figure 6. Voltage-dependent EL spectra of LT-Zn_3ppo_6 based devices (devices 3 and 4).

ethanol/CH_2Cl_2 (1:40) as the eluant to obtain 2-[(2-phenyl-2-hydroxyethyl)aminocarbonyl] ansiole (colorless solid, 8.8 g, yield 60%). ^{1}H NMR in $CDCl_3$ (δ, ppm): 8.44 (d, 1H), 7.98 (d, 1H), 7.40 (td, 2H), 7.0−7.2 (m, 2H), 4.02 (s, 3H).

Synthesis of 2-[(2-Phenyl-2-oxoethyl)aminocarbonyl]-ansiole. The Dess−Martin periodinane reagent[22] (10 g, 23.56 mmol) was added to a solution of 2-[(2-phenyl-2-hydroxyethyl)-aminocarbonyl]ansiole (5.96 g, 22 mmol) in dichloromethane (200 mL), and then stirred for 70 min at room temperature. $Na_2S_2O_3$ (10 g) and saturated $NaHCO_3$ aqueous solution were added slowly to the mixture. The organic layer was separated, washed with a saturated $NaHCO_3$ aqueous solution, dried ($MgSO_4$), evaporated, and then purified in a chromatographic column using hexane/EtOAc (4:1). Colorless solid, 5.8 g, yield 98%. ^{1}H NMR in $CDCl_3$ (δ, ppm): 8.44 (d, 1H), 7.98 (d, 1H), 7.40 (td, 2H), 7.0−7.2 (m, 2H), 4.02 (s, 3H).

Synthesis of 2-[(5-Phenyl-1,3-oxazolyl)ansiole. Triphenylphosphine (14.14 g, 54 mmol), hexachloroethane (12.76 g, 54 mmol), triethylamine (10.91 g, 107.8 mmol), and 2-[(2-phenyl-2-oxoethyl)aminocarbonyl]ansiole (5.8 g, 21.5 mmol) were added to dichloromethane (200 mL). The mixture was stirred for 2 h at room temperature. This mixture was washed with a saturated NH_4Cl aqueous solution and saturated $NaHCO_3$. The separated organic layer was dried ($MgSO_4$) and evaporated, and a colorless solid was obtained by column chromatography using hexane/ethyl acetate (4:1). Colorless solid, 4.5 g, yield 83%. ^{1}H NMR in $CDCl_3$ (δ, ppm): 8.44 (d, 1H), 7.98 (d, 1H), 7.40 (td, 2H), 7.0−7.2 (m, 2H), 4.02 (s, 3H).

Synthesis of 2-Hydroxyphenyl-5-phenyl-1,3-oxazole. LiI (6 g, 44.7 mmol) and 2-[(5-phenyl-1,3-oxazolyl)ansiole (4.5 g, 17.9 mmol) were added to γ-collidine (100 mL). The mixture was refluxed for 13 h. This mixture was filtered and the filtrate was added to an HCl aqueous solution (1M/L, 100 mL), then filtered. The residual solid was dissolved in EtOAC (30 mL) and concentrated, and a colorless solid was obtained by column chromatography using hexane/ethyl acetate (1:1). Colorless solid, 3.95 g, yield 93%. ^{1}H NMR in $CDCl_3$ (δ, ppm): 8.44 (d, 1H), 7.98 (d, 1H), 7.40 (td, 2H), 7.0−7.2 (m, 2H), 4.02 (s, 3H).

Synthesis of $(Znppo_2)_n$. 2-Hydroxyphenyl-5-phenyl-1,3-oxazole (3.9 g, 16 mmol) was dissolved in 20 mL of ethanol. After the solution was stirred for 5 min, $ZnOAc_2$ (1.7 g, 8 mmol) was added and the solution was then heated for 20 min at 60 °C. After the mixture was cooled to room temperature, the yellow precipitate was filtered to obtain the $Znppo_2$ complex (4.2 g, 97%). The $Znppo_2$ powder was purified by a train sublimation method. The structure of the $(Znppo_2)_n$ complex was confirmed by X-ray crystallographic analysis with a single crystal and elemental analysis was obtained from YANACO MT-5.

Syntheses of the Different Polymorphs and Monomer of $Znppo_2$ System. Different crystal phases were obtained by the train sublimation method by loading $(Znppo_2)_n$ powder in a quartz tube, which was heated at 360 °C, 1×10^{-3} Torr. Crystalline powders of $(Znppo_2)_n$ were found on the part at about 280 °C for M-$Znppo_2$, 310 °C for LT-Zn_3ppo_6, and 340 °C for HT-Zn_3ppo_6. Anal. Calcd. for $Zn_3C_{90}H_{60}N_6O_{12}$: C, 66.99; H, 3.75; N, 5.21. Found: C, 66.94; H, 3.58; N, 5.29 for HT-Zn_3ppo_6. Found: C, 66.57; H, 3.59; N, 5.23 for LT-Zn_3ppo_6. For both oligomeric systems, mp 354 °C.

Single-Crystal X-ray Analysis of HT-Zn_3ppo_6. A yellow platelet crystal of $C_{90}N_6O_{12}H_{60}Zn_3$ having approximate dimensions of 0.06 × 0.20 × 0.40 mm was mounted on a glass fiber. The data were collected at a temperature of 23 °C to a maximum 2θ value of 50.7°. A total of 74 oscillation images were collected. A sweep of data was done using ω scans from 130.0 to 190.0° in 3.0° steps, at $\chi = 45.0°$ and $\phi = 0.0°$. The exposure rate was 300.0 [s/°]. A second sweep was performed using ω scans from 0.0 to 162.0° in 3.0° steps, at $\chi = 45.0°$ and $\phi = 180.0°$. The exposure rate was 300.0 [s/°]. The linear absorption coefficient, μ, for Mo Kα radiation is 11.0 cm^{-1}. Its application resulted in transmission factors ranging from 0.89 to 0.97. The data were corrected for Lorentz and polarization effects.

Single-Crystal X-ray Analysis of LT-Zn_3ppo_6. A yellow prism crystal of $C_{90}N_6O_{12}H_{60}Zn_3$ having approximate dimen-

(22) Dess, D. B.; Martin, J. C. *J. Am. Chem. Soc.* **1991**, *113*, 7277.

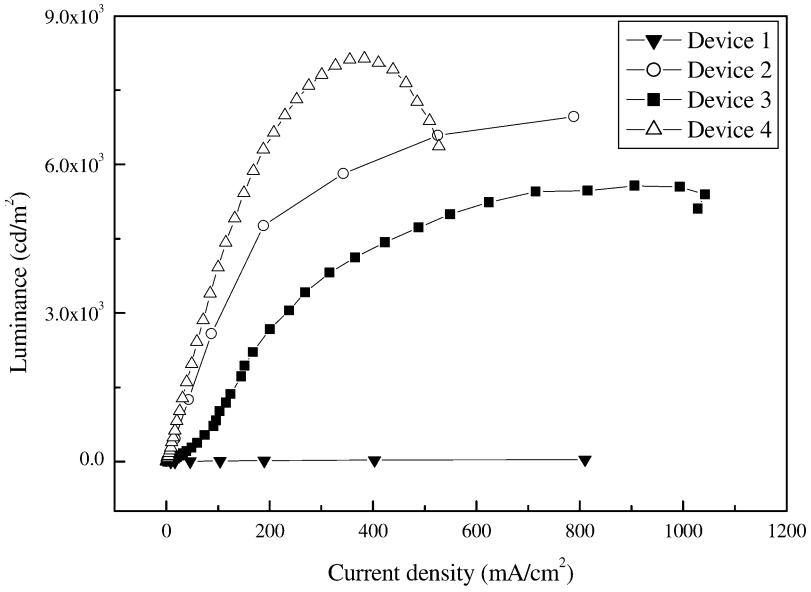

(a) Luminance-current density characteristics.

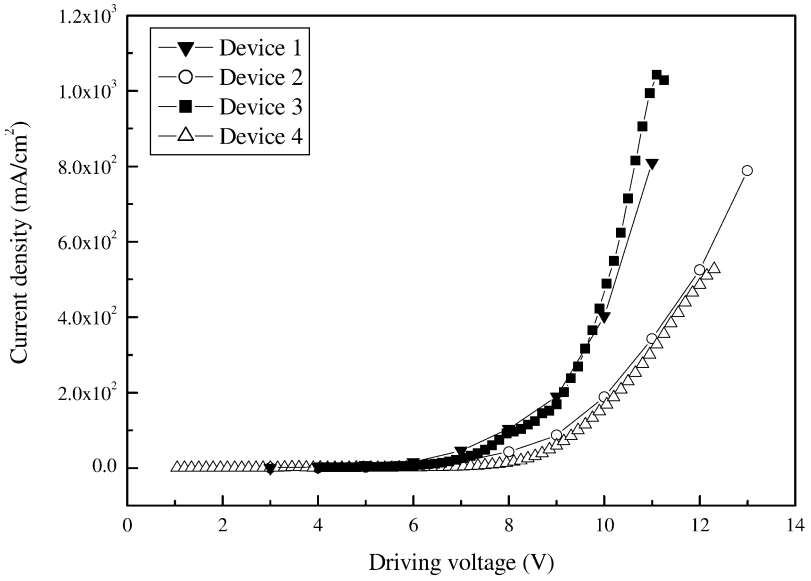

(b) Current density-voltage characteristics.

Figure 7. EL characteristics of OLEDs using Zn_3ppo_6 as an emitting layer.

sions of 0.10 × 0.10 × 0.10 mm was mounted on a glass fiber. The data were collected at a temperature of 23 °C to a maximum 2θ value of 54.8°. A total of 85 oscillation images were collected. A sweep of data was done using ω scans from 130.0 to 190.0° in 2.0° steps, at $\chi = 45.0°$ and $\phi = 0.0°$. The exposure rate was 600.0 [s/°]. A second sweep was performed using ω scans from 0.0 to 165.0° in 3.0° steps, at $\chi = 45.0°$ and $\phi = 180.0°$. The exposure rate was 600.0 [s/°]. Of the 16 204 reflections that were collected, 7791 were unique ($R_{int} = 0.092$); equivalent reflections were merged. The linear absorption coefficient, μ, for Mo Kα radiation is 11.0 nm^{-1}. Its application resulted in transmission factors ranging from 0.45 to 1.46. The data were corrected for Lorentz and polarization effects.

Single-Crystal X-ray Analysis of M-Znppo₂. A pale yellow needle crystal of $C_{30}N_2O_4H_{20}Zn$ having approximate dimensions of 0.04 × 0.05 × 0.20 mm was mounted on a glass fiber. The data were collected at a temperature of 23 ± 1 °C to a maximum 2θ value of 50.7°. A total of 105 oscillation images were collected. A sweep of data was done using ω scans from 130.0 to 190.0° in 2.0° steps, at $\chi = 45.0°$ and $\phi = 0.0°$. The exposure rate was 600.0 [s/°]. A second sweep was performed using ω scans from 0.0 to 158.0° in 2.0° steps, at $\chi = 45.0°$ and $\phi = 180.0°$. The exposure rate was 600.0 [s/°]. The crystal-to-detector distance was 127.40 mm. Of the 5244 reflections that were collected, 3489 were unique ($R_{int} = 0.106$); equivalent reflections were merged. No decay correction was applied. The linear absorption coefficient, μ, for Mo Kα radiation is 10.8 cm^{-1}. Its application resulted in transmission factors ranging from 0.57 to 1.48. The data were corrected for Lorentz and polarization effects.

Fabrication of OLEDs. The organic EL devices using Zn_3ppo_6 as an emitting layer were fabricated on an indium−tin oxide (ITO with a sheet resistance of 10 Ω/cm^2) substrate. The organic layers and LiF were successively deposited onto ITO glass under 3 × 10^{-6} Torr. Next, aluminum cathode with a thickness of 100 nm was deposited onto the LiF layer under 3 × 10^{-6} Torr. The deposition rate of organic layers and the metallic cathode were 0.4 and 0.8 nm/s, respectively. *N*, *N*′-diphenyl-*N*,*N*′-bis-(3-methyl-phenyl)-[1,1′-biphenyl]-4,4′- diamine (TPD) was used as a hole transport layer with a thickness of 48 nm for device 4, whereas a 50-nm thickness

was used for other devices. 2-(4-Biphenylyl)-5-(*tert*-butylphenyl)-1,2,3-oxadiazole (PBD) was used as a hole-blocking layer.

Acknowledgment. We thank Mr. A. Takashima of Ya-Man Ltd. for the refractive index measurement.

Supporting Information Available: Crystallographic information files (CIF) for monomer, LT-Zn_3ppo_6, and HT-Zn_3ppo_6. This material is available free of charge via the Internet at http://pubs.acs.org.

CM0346428